Nanoscale Res Lett (2009) 4:921–925
DOI 10.1007/s11671-009-9336-4

NANO EXPRESS

Magnetoresistance in Sn-Doped In_2O_3 Nanowires

Olívia M. Berengue · Alexandre J. C. Lanfredi · Livia P. Pozzi · José F. Q. Rey · Edson R. Leite · Adenilson J. Chiquito

Received: 12 February 2009 / Accepted: 24 April 2009 / Published online: 4 July 2009

Abstract In this work, we present transport measurements of individual Sn-doped In_2O_3 nanowires as a function of temperature and magnetic field. The results showed a localized character of the resistivity at low temperatures as evidenced by the presence of a negative temperature coefficient resistance in temperatures lower than 77 K. The weak localization was pointed as the mechanism responsible by the negative temperature coefficient of the resistance at low temperatures.

Keywords Oxide nanowires · Weak localization · Electron transport · Electron–electron scattering

Introduction

Quasi 1D metal oxide nanostructures have attracted considerable interest in the last years for fundamental studies and also for potential applications. In particular, they present properties which range from metals to semiconductors and insulators [1]: the performance of these devices is strongly correlated to their structural and electronic properties. These low-dimensional structures have been used as building blocks in different devices and nanodevices [2] and they are important for both fundamental research and applications because they have the potential to reach high device integration. One of the most prominent applications of these materials is the gas sensing devices [3–5], but this and other potential electronic applications of nanowires still require a detailed understanding of their fundamental electronic properties [6].

Although these nanostructures be usually grown by self-organized processes like the vapor–liquid–solid mechanism (VLS) [7] and thus presenting a high crystalline quality, some disorder is always present. In this way, electrons subjected to a random potential are not able to move freely through the system if either potential fluctuations due to disorder exceed a critical value or the electron energy is lower than the characteristic potential fluctuation [8, 9]. It is interesting to add that the carrier localization should be evidenced in one-dimensional structures as stated by the Anderson's localization theory: it predicts that disorder in these systems leads to carrier's localization.

In this work we present some transport measurements of individual Sn-doped In_2O_3 nanowires as a function of temperature and magnetic field. The results showed a localized character of the resistivity at low temperatures as evidenced by the presence of a negative temperature coefficient resistance in temperatures lower than 77 K. This behavior was successfully associated to weak localization picture where the boundary scattering processes provide the main inelastic scattering mechanism.

O. M. Berengue (✉) · L. P. Pozzi · A. J. Chiquito
Departamento de Física, Universidade Federal de São Carlos, CEP 13565-905, CP 676 São Carlos, São Paulo, Brazil
e-mail: oliberengue@yahoo.com.br

A. J. C. Lanfredi · J. F. Q. Rey
Centro de Engenharia, Modelagem e Ciências Sociais Aplicadas, Universidade Federal do ABC, CEP 09210-170, Santo André, São Paulo, Brazil

E. R. Leite
Laboratório Interdisciplinar de Eletroquímica e Cerâmicas, Departamento de Química, Universidade Federal de São Carlos, CEP 13565-905, CP 676 São Carlos, São Paulo, Brazil

Experimental

The samples used here were grown by the well-known VLS growth mechanism in association with a carbothermal reduction process [10, 11]. For this purpose In_2O_3 and SnO_2 powders (purity >99.9%) were mixed with 10% in weight of carbon black and each mixture was placed inside a horizontal tube furnace in two separated alumina crucibles. The synthesis was carried out at 1150 °C under a N_2 gas flux of 50 sccm for 4 h.

The wooly-like collected material was analyzed by X-ray diffraction (XRD) as plotted in Fig. 1a. It was possible to identify the cubic In_2O_3 structure by the crystallographic indices (PDF 6-416). Also, it could be identified the Sn and SnO_2 structures as an evidence of the self-catalytic VLS growth mechanism.

To improve the structural characterization of the samples, a transmission electron microscopy (TEM; Jeol model JEM 2100 operating at 200 kV) was carried out on individual ITO nanowires. Figure 1b shows a low-magnification TEM image of an individual nanowire with 200 nm width. In order to study the orientation growth and high crystallinity of the samples, a high resolution TEM image (HRTEM) was performed at the end of the nanowire and it is shown in Fig. 1c. After a fast Fourier transform (FFT) of the HRTEM image, by using an image analysis software, it was obtained a point matrix which is the frequency spectrum, sketched in Fig. 1d. The points showed in this equivalent SAED (selected-area electron diffraction) image allow the indexing of the growth direction to be [100] and are in agreement with interatomic distances measured. This plane growth direction is in accordance with the XRD pattern plotted in Fig. 1a, which shows the [400] peaks intensity higher than the obtained from bulk materials.

The Raman characterization was performed in order to identify the ITO vibrational modes and confirms the XRD results. The micro-Raman experiments were carried out at room temperature with a T 64000 Jobin Yvon spectrometer using the 514.5 nm line of an argon ion laser as excitation source. The power was kept below 5 mW to avoid overheating. Figure 2 shows the Raman spectra of the wooly-like material. It is known that the body-centered cubic In_2O_3 belongs to the space group Ia_3, Th_7 [12]. For such a structure, the vibrations with symmetry A_g, E_g, and T_g are Raman active giving rise to 22 Raman modes. Five Raman peaks at 112, 133, 303, 491, and 616 cm^{-1} were found to belong to the vibrational modes of the bcc-In_2O_3, which seems to be in good agreement with the reported values in the literature [13]. The other peaks are probably related to the presence of Sn atoms in In sites of In_2O_3 leading to different vibrational modes. The ITO vibrational features are now under study and will be the subject of a new paper.

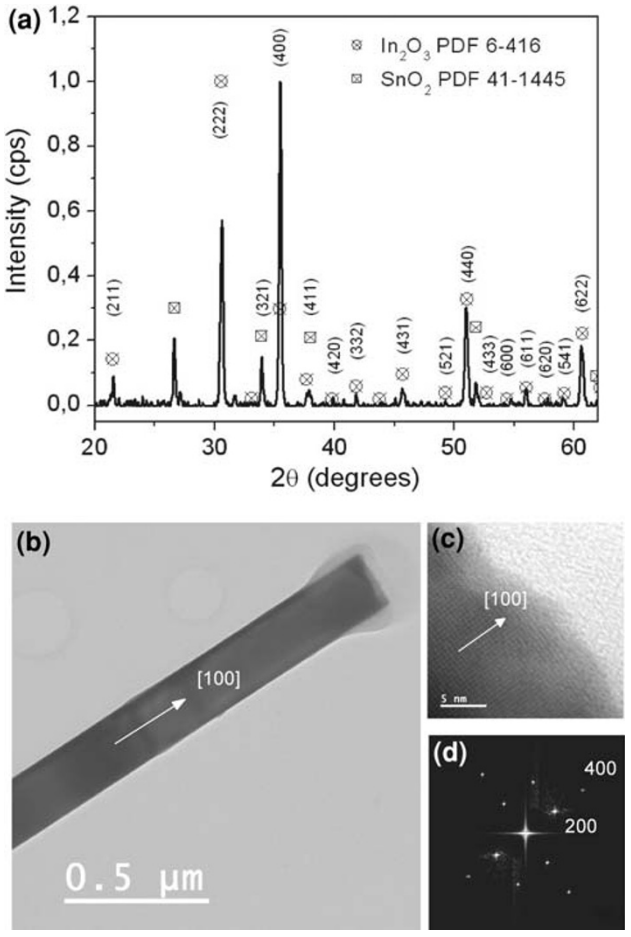

Fig. 1 **a** X-ray diffraction pattern of the as grown material; **b** low-magnification TEM image of an ITO nanowire; **c** HRTEM image of the end of the same nanowire; **d** fast Fourier transform of the image shown in panel **b**

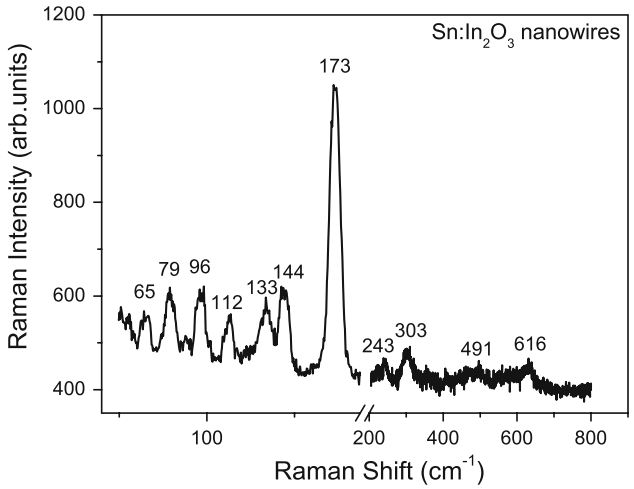

Fig. 2 Raman spectrum taken at room temperature showing the expected phonon modes for bcc-In_2O_3

After the structural characterization, the samples were prepared for the contacts' fabrication. The samples were then ultrasonically dispersed in ethanol and were placed onto an oxidized Si wafer (300 nm of SiO_2 layer) with metallic (Au/Ni, 100 nm thickness) pads. The transport measurements were carried out using standard low frequency ac lock-in techniques, at 13 Hz. The low temperature data were obtained using a closed cycle helium cryostat at a base pressure 5×10^{-6} Torr.

Results and Discussion

Samples with 68–70 nm width were used for transport measurements. The resistance-temperature dependent measurements were conducted with B = 0 and using different current levels (from 0.1 to 10 μA) but the results remain unchanged (Fig. 3). In the high temperatures range, 77–300 K, the nanowires exhibit a positive temperature coefficient of resistance and a weak temperature dependence, a typical metal-like character. It is interesting to add that the metallic behavior was found in other and larger samples (see the inset in Fig. 3) and it is present even at the lowest used temperature, T = 10 K. Since the ITO nanowires are expected to remain metallic, the carrier density is a weak function of temperature and the resistance should be mainly determined by the temperature dependence of the various scattering mechanisms through electrons' mobility [6]. At high temperatures ($T > 77$ K), the phonon scattering seems to be dominant and the resistance rises with increasing temperature (metallic phase).

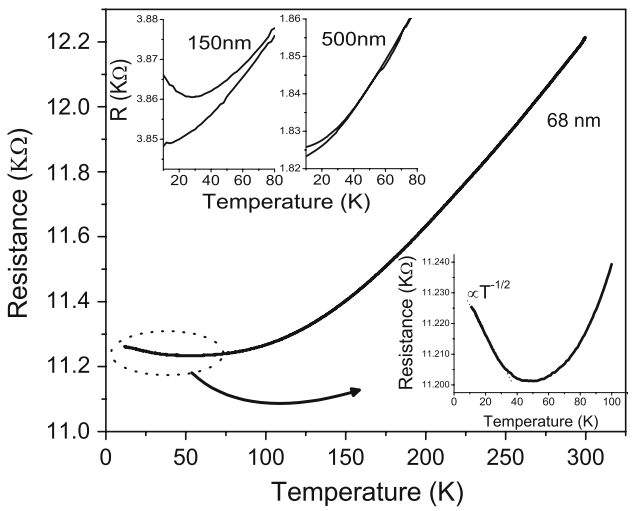

Fig. 3 Resistance-temperature dependent measurements taken at B = 0 and using different current levels (only 1 μA is shown). In the high temperatures range, the nanowires exhibit a positive temperature coefficient of resistance and a weak temperature dependence. The inset shows the results for other and larger samples showing the same behavior

These resistance data were analyzed in the framework of the Bloch–Grüneisen theory (based on the electron-acoustic phonon scattering mechanism) due to the observed metallic character. In this way, the resistance is described by [14]

$$R(T) = R_0 + A\left(\frac{T}{\Theta_D}\right)^n \int_0^{\Theta_D/T} \frac{z^n e^z}{(e^z - 1)^2} dz \quad (1)$$

where A is a parameter proportional to the electron–phonon coupling and R_0 is the residual resistance; n usually ranges from 3 to 5 when the electron–phonon interaction is mainly responsible for the scattering events [14]; Θ_D is the Debye temperature. The fitting of the experimental data using Eq. 1 revealed $n = 3.6$ and $\Theta_D = 1227$ K: as the temperature and phonon excitation increase, the amount of scattering events experienced by the conduction electrons are increased as well, resulting in a greater resistivity (theoretical value of $\Theta_D = 1200$ K). It is interesting to add that the Bloch–Grüneisen theory can be only used in the range of nanowires' size where the electron-acoustic phonon scattering remains unchanged as pointed in Ref. [15].

The analysis for the low temperature data is more challenging: down from 77 K the sample's resistance increases indicating that a different transport and scattering mechanisms are acting in this range of temperatures. The observed negative temperature coefficient resistance could not be fitted to an usual activation (exponential) law. However, it preserves the localized character for electron transport. As reported in literature for Zn [16] and Sb [17] nanowires, we also found that the resistivity increase follows essentially a $T^{-1/2}$ law (the equation $R = 0.01 + 6.7 \times 10^{-4}/\sqrt{28 + T}$ fits well the temperature dependence shown in Fig. 3). The observation of an *exact* $T^{-1/2}$ law should be unambiguously attributed to a signature of the presence of electron–electron inelastic scattering mechanism [18]. Simple activated and one-dimensional hopping laws were used and discarded because they lead us to wrong results. Then, a more detailed analysis is needed including, for instance, the presence of carriers' localization and other scattering mechanisms.

As observed in literature [6, 19–21] for small-dimension nanowires, processes like collisions with the boundaries provide disorder, which in turn randomizes the electron energy and increases the electron–electron interaction. These interactions are also expected to contribute to the transport leading to an increase of the resistance since the diffusive motion of the electrons enhances their interactions.

In our case, taking into account the nanowire's cross section, the boundary scattering (mostly temperature independent) becomes an important inelastic scattering

mechanism at low temperatures leading to a finite size effect. As a result, a localized character for the electron's transport is achieved. Then, the observed negative temperature coefficient can be interpreted as a result of the mixture of the two scattering process (electron–electron and boundary collisions) at low temperatures, both leading to a localization character for the electron transport. This effect can be studied by using magnetoresistance experiments.

Independently of the main mechanism of inelastic scattering of electrons, the phase-breaking time and length are power functions of temperature leading to a quantum correction for conductivity/resistivity which is quantified by the weak localization in a form $\Delta R \propto \ln T$. Unfortunately, the electron–electron interaction produces the same dependence on the temperature. In order to establish the mechanism responsible by the increase of the resistivity, we conducted resistance measurements under different magnetic fields. The weak localization is known by the highly sensibility to a weak magnetic field. Figure 4a shows the linear dependence of resistance as function of the ln T and for different magnetic field intensities. From these curves we see that the expected ln T dependence of the resistivity is clearly observed until $\sim$0.3 T when the magnetic field is strong enough to break the quantum interference. For higher magnetic fields, the resistance does not exhibit the negative temperature coefficient (also, the larger samples do not show any dependence on the magnetic field, as expected).

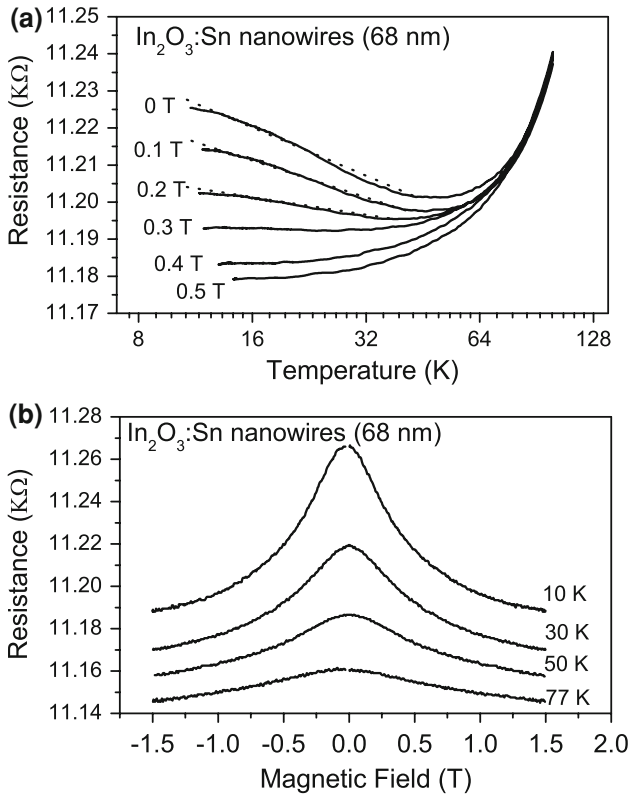

Fig. 4 **a** The linear dependence of resistance as function of the ln T and for different magnetic field intensities. The expected ln T dependence of the resistivity is clearly observed until $\sim$0.3 T and for higher magnetic fields, the resistance does not exhibit the negative temperature coefficient. **b** The magnetoresistance measurements providing additional confirmation of weak localization effects

Additional confirmation of weak localization effects was obtained by magnetoresistance measurements as seen in Fig. 4b. From these measurements we calculated the phase-breaking length ($L_\phi = 72$ nm). From the theory, the critical B field needed to suppress the weak localization is given by

$$B_C = \frac{h}{qWL_\phi}, \tag{2}$$

where W is the width of the wire [22]. Using the results presented in Fig. 4, one finds $B_C = 0.84$ T: below this value the weak localization regime should determine the behavior of the conductivity of the sample, as observed.

This result is twofold: first, the weak localization is suppressed at high B fields as expected and confirming that the negative temperature coefficient is a result of the disorder-induced localization. Second, it indirectly gives an evidence of a transition from one-dimensional (weak field) to three-dimensional localization (high field). In fact, for weak fields the magnetic length $L_B(=\sqrt{\hbar/eB})$ is greater than the width of the samples and L_ϕ: from the viewpoint of the electrons, the nanowire is an one-dimensional system. Otherwise, the nanowire behaves essentially like a three-dimensional system. In both cases, the disorder coming from the boundary scattering plays the fundamental role giving the main scattering mechanism for the diffusive electron transport.

Conclusion

Electronic properties of self-assembled high crystalline quality tin-doped indium oxide were studied. We report on the experimental data and the related analysis on the resistance and magnetoresistance of these single crystal nanowires. The weak localization was pointed as the mechanism responsible by the negative temperature coefficient of the resistance at low temperatures. From the magneto-resistance data we quantified the characteristic phase-breaking length of the system; additionally, we observed a three- to one-dimensional transition for the localization character of the resistance.

Acknowledgment The authors thank the Brazilian research funding Agencies FAPESP and CNPq for the financial support of this work.

References

1. Z. Pan, Z. Dai, Z. Wang, Science **291**, 1947 (2001)
2. X. Duan, Y. Huang, Y. Cui, J. Wang, C.M. Lieber, Nature **409**, 6649 (2001)
3. J. Kappler, A. Tomescu, N. Barsan, U. Weimar, Thin Solid Films **391**, 186 (2001)
4. M. Radecka, J. Przewoznik, K. Zakrzewska, Thin Solid Films **39**, 247 (2001)
5. C. Li, D. Zhang, S. Han, X. Liu, T. Tang, C. Zhou, Adv. Mater.**15**, 143 (2003)
6. A.J. Chiquito, A.J.C. Lanfredi, R.F.M. Oliveira, L.P. Pozzi, E.R. Leite, Nanoletters **7**, 1439 (2007)
7. R.S. Wagner, W.C. Ellis, Appl. Phys. Lett. **4**, 89 (1964)
8. Yu.A. Pusep, A.J. Chiquito, S. Mergulhão, A.I. Toropov, J. Appl. Phys. **92**, 3830 (2002)
9. A.J. Chiquito, Yu.A. Pusep, G.M. Gusev, A.I. Toropov, Phys. Rev. B **66**, 035323 (2002)
10. E.R. Leite, J.W. Gomes, M.M. Oliveira, E.J.H. Lee, E. Longo, J.A. Varela, C.A. Paskocimas, T.M. Boschi, F. Lanciotti, P.S. Pizani, P.C. Soares, J. Nanosci. Nanotechnol. **2**, 125 (2002)
11. M.O. Orlandi, R. Aguiar, A.J.C. Lanfredi, E. Longo, J.A. Varela, E.R. Leite, Appl. Phys. A **80**, 23 (2005)
12. W.B. White, V.G. Keramidas, Spectrochim. Acta **28A**, 501 (1972)
13. H. Sobotta, H. Neumann, G. Kühn, V. Riede, Cryst. Res. Technol. **25**, 61 (1990)
14. J.M. Ziman, *Electrons and Phonons* (Claredon Press, Oxford, 1960)
15. A. Bid, A. Bora, A.K. Raychaudhuri, Phys. Rev. B **74**, 035426 (2006)
16. J.P. Heremans, C.M. Thrush, D.T. Morelli, M.C. Wu, Phys. Rev. Lett. **91**, 076804 (2003)
17. Y. Zhang, L. Li, G.H. Li, L.D. Zhang, Phys. Rev. B **73**, 113403 (2006)
18. D.E. Beutler, N. Giordano, Phys. Rev. B **8**, 38 (1988)
19. T.J. Thornton, M.L. Roukes, A. Scherer, B.P. Van der Gaag, *Granular Nanoelectronics*, ed. by D.K. Ferry, J.R. Baker, C. Jacobon, NATO ASI Series (Plenum Press, New York, 1991)
20. W. Wu, S.H. Brongersma, M. Van Hove, K. Maex, Appl. Phys. Lett. **84**, 2838 (2004)
21. H. Kind, H. Yan, B. Messer, M. Law, P. Yang, Adv. Mater. **14**, 158 (2002)
22. S. Datta, *Electronic Transport in Mesoscopic Systems* (Cambridge University Press, Cambridge, 1997)